Catalysis

Ruthenium Nanoparticles Supported on Reduced Graphene Oxide: Efficient Catalyst for the Catalytic Reduction of Cr (VI) in the Presence of Amine-Boranes

Mehmet Yurderi,[a] Ahmet Bulut,[a] Gulsah Saydan Kanberoglu,[a] Murat Kaya,[b] Yasin Kanbur,[c] and Mehmet Zahmakiran*[a]

Hexavalent chromium (Cr(VI)) is a toxic, mutagen and carcinogen contaminant exist in surface and groundwater, while its reduced form trivalent chromium (Cr(III)) is known as an essential element to normal carbohydrate, lipid and protein metabolism in nature. Addressed herein, for the first time, ruthenium nanoparticles supported on reduced graphene oxide (Ru@rGO) catalyze the reduction of aqueous Cr(VI) to Cr (III) in the presence of amine-boranes; ammonia-borane (AB; NH_3BH_3), methylamine-borane (MeAB; $CH_3NH_2BH_3$), dimethylamine-borane (DMAB; $(CH_3)_2NHBH_3$) as reducing agents under mild conditions (at room temperature and under air). Ru@rGO catalyst was reproducibly fabricated through a double-solvent method followed by wet-chemical reduction and characterized by using various spectroscopic and visualization techniques, which showed that the formation of well-dispersed and highly crystalline ruthenium(0) nanoparticles with a mean particle size of 2.7 ± 0.9 nm on the surface of rGO. The catalytic performance of Ru@rGO was investigated in terms of activity and stability in the ammonia-borane assisted reduction of Cr(VI) to Cr(III), and the sum of the results gained from these catalytic tests revealed that Ru@rGO acts as both active (TOF = 7.6 mol $Cr_2O_7^{2-}$/mol Ru.min) and stable (80% of its initial activity at 90% conversion at 5th reuse) heterogeneous catalyst in this significant catalytic transformation. This study also reports kinetic studies for Ru@rGO catalyzed Cr(VI) reduction in the presence of ammonia-borane depending on ruthenium ([Ru]), ammonia-borane ([AB]) concentrations and temperature to shed some light on the nature of the catalytic reaction and activation parameters.

Introduction

Hexavalent chromium (Cr(VI)) is known as the second most abundant heavy metal contaminant exists in the surface and groundwater[1] and is mainly produced from electroplating, pigment manufacturing, tannery facilities, and wood preservation.[2–5] More importantly, Cr(VI) is carcinogenic to humans and can cause dermatitis, rhinitis even lung cancer, and nasopharynx cancer.[6,7] Cr(VI) is highly mobile in an aqueous environment, and the mobile form of Cr(VI) has the potential for increased exposure and harm to human health and the environment.[8] In contrast, the reduced form of chromium, trivalent chromium Cr(III), is less mobile in the environment and much less toxic. Indeed, trace amounts of Cr (III) is an essential nutrient for living organisms.[9,10] Henceforth, the reduction of Cr(VI) to Cr(III) is environmentally favorable and can be used to remediate Cr(VI) contaminated sites. In this context, various reducing agents, including H_2S, Fe^{2+}, H_2, and HCOOH, have been tested for the reduction of Cr(VI) to Cr (III).[11–14]

Amongst these reduction processes, the notable performances have been achieved by using transition metal nanoparticles as a catalyst and formic acid (HCOOH) as a reducing agent.[14] In these catalytic transformations, formic acid undergoes dehydrogenation reaction (**1**) in the presence of a suitable catalyst.[15–18] Then, H_2 adsorbed on the surface of active metal nanoparticles subsequently reduces Cr(VI) to Cr(III) via an H_2 transfer pathway (**2**).[19,20] The most significant drawbacks in the formic acid assisted the reduction of Cr(VI) is (*i*) slow reaction kinetics and (*ii*) the limitation in the use of different transition metals as active catalytic species, which are mainly palladium-based catalysts, due to the selectivity problem in formic acid decomposition.[17,21,22] Formic acid decomposes in two different ways; these are dehydrogenation (**1**), and dehydration (**3**) pathways.[17]

$$HCOOH \rightarrow H_2 + CO_2 \quad (1)$$

$$Cr_2O_7^{2-} + 8H^+ + 3H_2 \rightarrow 2Cr^{3+} + 7H_2O \quad (2)$$

$$HCOOH \rightarrow H_2O + CO \quad (3)$$

[a] *M. Yurderi, A. Bulut, Dr. G. S. Kanberoglu, M. Zahmakiran*
Nanomaterials and Catalysis Research Group, Department of Chemistry, Van Yuzuncu Yil University, 65080, Van, Turkey
E-mail: zmehmet@yyu.edu.tr
[b] *M. Kaya*
Department of Chemical Engineering and Applied Chemistry, Atilim University, 06836, Ankara, Turkey
[c] *Dr. Y. Kanbur*
Department of Metallurgical and Materials Engineering, Karabuk University, 78050, Karabuk, Turkey

Supporting information for this article is available on the WWW under https://doi.org/10.1002/slct.202001380

© 2020 Wiley-VCH Verlag GmbH & Co. KGaA, Weinheim

The dehydration of formic acid is the unwelcome reaction and cannot assist the reduction of Cr(VI). The surveying of the catalytic systems used in formic acid dehydrogenation showed that the majority of these catalytic systems are composed of active palladium (Pd) species, which reveal the highest dehydrogenation selectivity in formic acid decomposition. At this concern, the development of new catalytic reduction processes for Cr(VI) reduction that provides fast reaction kinetics and allowing the employment of wide-range transition metals has great importance in this catalytic transformation.

In this study, for the first time, we report ruthenium nanoparticles supported on reduced graphene oxide (Ru@rGO) catalyze the reduction of aqueous Cr(VI) to Cr(III) in the presence of amine-boranes; ammonia-borane (AB; NH_3BH_3), methylamine-borane (MeAB; $CH_3NH_2BH_3$) and dimethylamine-borane (DMAB; $(CH_3)_2NHBH_3$) used as reducing agents. Hydrogen can be generated from these amine-boranes through their catalytic hydrolysis reactions (**4**-**6**).[23–25]

$$NH_3BH_3 + 2H_2O \rightarrow NH_4BO_2 + 3H_2 \quad (4)$$

$$CH_3NH_2BH_3 + 2H_2O \rightarrow CH_3NH_3BO_2 + 3H_2 \quad (5)$$

$$(CH_3)_2NHBH_3 + 2H_2O \rightarrow (CH_3)_2NH_2BO_2 + 3H_2 \quad (6)$$

Ruthenium nanoparticles supported on reduced graphene oxide (Ru@rGO) were prepared through a double-solvent method[26,27] followed by wet-chemical reduction technique[28] and characterized by using various analytical techniques including inductively coupled plasma optical emission spectroscopy (ICP-OES), X-ray photoelectron spectroscopy (XPS), powder X-ray diffraction (P-XRD), field emission scanning electron microscopy (FE-SEM), transmission electron microscopy (TEM), high resolution transmission electron microscopy (HRTEM) and scanning transmission electron microscopy-energy dispersive X-ray spectroscopy (STEM-EDX). The results gained from these analyses revealed that the formation of well-dispersed and highly crystalline ruthenium nanoparticles with a mean particle size of 2.7 ± 0.9 nm on the surface of rGO. The catalytic studies performed on Cr(VI) reduction by using Ru@rGO catalyst showed that it provides remarkable activity in the catalytic Cr(VI) reduction in the presence of AB with an initial turnover frequency value of TOF = 7.6 mol $Cr_2O_7^{2-}$/mol Ru.min, which is the highest activity value reported for Cr(VI) reduction in the literature (*vide infra*). Moreover, these rGO supported ruthenium nanoparticles display notable durability against to leaching and sintering throughout the catalytic runs, which makes them highly reusable catalyst for this catalytic transformation, they preserve almost their inherent catalytic performance (80% of its initial activity at 90% conversion) at 5th catalytic reuse in the catalytic Cr(VI) reduction.

Results and Discussion

Ruthenium nanoparticles supported on reduced graphene oxide were prepared reproducibly by following two-steps procedure comprising of a double-solvent method[26,27] to impregnate $RuCl_3.3H_2O$ precatalyst on reduced graphene oxide surface then their wet-chemical-reduction[28] by using sodium borohydride ($NaBH_4$). The dark-gray solid powdered samples of Ru@rGO yielded and isolated at the end of the synthesis protocol were characterized by multiple analytical techniques. First, to find the amount of ruthenium deposited on the surface of rGO, ICP-OES analysis was carried out, and the ruthenium content of as-prepared Ru@rGO was found to be 1.2% wt. Next, P-XRD analyses were performed on graphene oxide (GO), reduced graphene oxide (rGO) and Ru@rGO (contains 1.2 wt % Ru), and P-XRD patterns of these materials are given in Figure 1. The characteristics carbon peak (001) for GO seemed at 11.2° corresponding to definite *d*-spacing of 0.8 nm as reported by Marcano and co-workers.[29] After hydrazine reduction of GO, (001) peak ultimately disappear and the new Bragg peak (002) was observed at 25.1°, matching to the of the interlayer distance of 0.4 nm that is very consistent with the previously reported[30] and revealed the good arrangement of the

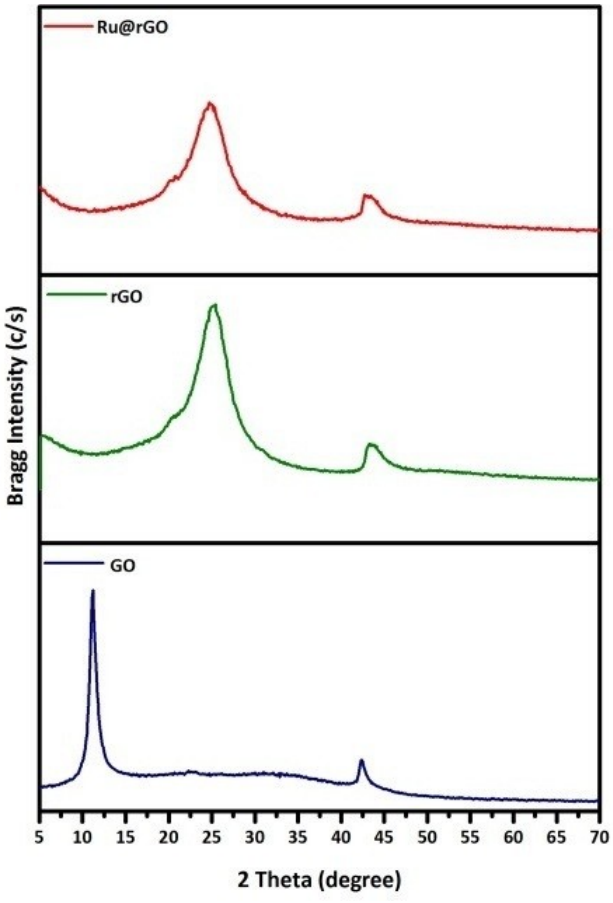


Figure 1. Powder X-ray diffraction (P-XRD) patterns of graphene oxide (GO), reduced graphene oxide (rGO), and ruthenium nanoparticles supported on reduced graphene oxide (Ru@rGO) in the range of 2θ = 5-70°.

© 2020 Wiley-VCH Verlag GmbH & Co. KGaA, Weinheim

interlayer distance of graphene. On the other hand, a P-XRD pattern of Ru@rGO was found to be identical with that of rGO. The absence of any Bragg peaks assignable to ruthenium nanoparticles can be ascribed to their low amount of loading ($<$ 10 wt %) onto rGO. Additionally, it should also be noted that, we realized that the most notable diffraction line of metallic ruthenium; Ru (101), which was also seen by HRTEM image, overlaps with Bragg peak of rGO (102) plane at around 43° (**Figure S1**). As well, the decrease in Bragg peak intensities in Ru@rGO sample can be elucidated by the changes in the charge distribution and electrostatic fields as a result of the existence of ruthenium nanoparticles on the surface and interaction of their electrophilic surface with rGO atoms.[31]

The oxidation state of ruthenium nanoparticles and the surface elemental analysis of Ru@rGO (1.2 wt % Ru loading) were examined by XPS analyses. The survey XPS spectrum of Ru@rGO is depicted in Figure 2(a), which shows the existence of ruthenium as well as rGO elements (carbon, oxygen). The existence of sodium (Na) signal indicative of the presence of surface-bound contaminated sodium (Na^+) ions came from sodium borohydride ($NaBH_4$), which was used as a reducing agent. The high resolution (HR-XPS) spectrum of Ru@rGO sample (1.2 wt % Ru loading) at Ru 3p core level and its deconvolutions are given in Figure 2(b). The deconvolutions of

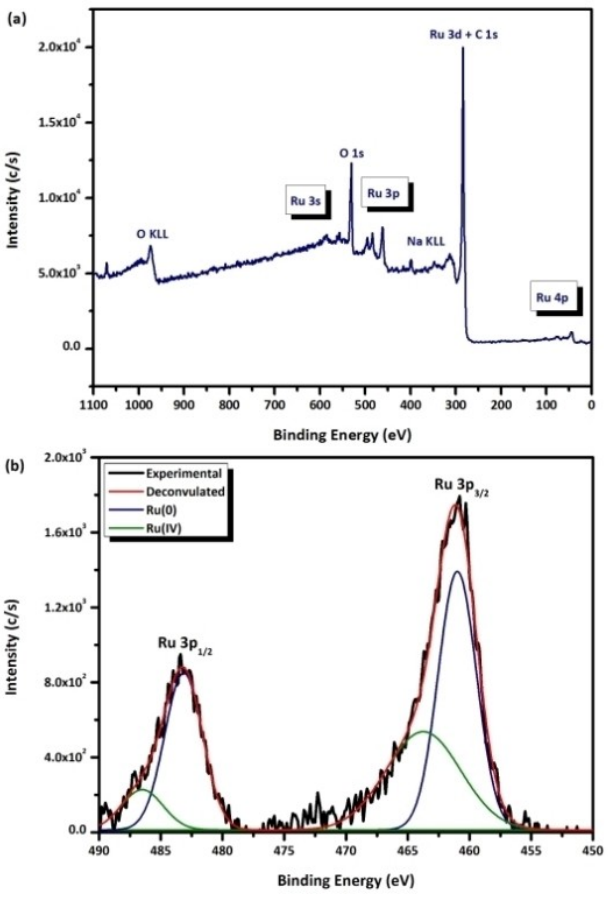


Figure 2. (a) Survey XPS spectrum of Ru@rGO, (b) Ru 3p core-level high resolution XPS spectrum of Ru@rGO.

high-resolution Ru 3p XPS spectrum of Ru@rGO sample gives distinguishing peaks at 483.2 and 461 eV, which can readily be assigned to $3p_{1/2}$ and $3p_{3/2}$ peaks of metallic Ru(0).[48,49] The additional low-intensity peaks observed at 486.5 and 463.7 eV discloses the presence of RuO_2 phase, which may originate from the surface oxidation of ruthenium nanoparticles during the XPS sampling procedure.[32]

FE-SEM, TEM, HRTEM, and STEM-EDX analyses were performed on Ru@rGO sample (1.2 wt % Ru loading) to examine the size, morphology, and the composition of Ru@rGO (1.2 wt % Ru loading). FE-SEM images of Ru@rGO in different magnification are given in Figure 3, which exhibits stacked plates of rGO and no bulk Ru formation in observable size. Although no bulk ruthenium is seen on the surface of rGO support material, ICP-OES and STEM-EDX mapping (Figure 3(e)) analyses reveal that the presence of ruthenium in the analyzed Ru@rGO sample, which entails that the formation of small-sized ruthenium nanoparticles.

Indeed, TEM images of Ru@rGO sample (1.2 wt % Ru loading) given in Figure 4(a)–(b) display the existence of well-dispersed and small-sized ruthenium (0) nanoparticles on the surface of rGO, the mean particle size of the resulting surface-bound ruthenium(0) nanoparticles was found to be 2.7 $\pm$ 0.9 nm by the particle size analysis of $>$ 50 non-touching particles. In addition to the size and dispersion, the crystallinity of the resulting ruthenium nanoparticles was also examined by HRTEM analysis and the HRTEM image of Ru@rGO sample is given in Figure 4(c), which show the formation of highly crystalline ruthenium nanoparticles with a crystalline spacing of 0.22 nm, that agrees with the (101) lattice spacing of ruthenium.[33] The surface elemental composition of the resulting Ru@rGO was investigated STEM-EDX spectroscopy, and STEM-EDX spectrum of Ru@rGO is depicted in Figure 4(d), which shows the existence of ruthenium in the analyzed regions (copper arose from carbon-coated copper TEM grid).

The catalytic performance of Ru@rGO catalyst was examined in the catalytic reduction of Cr(VI) to Cr(III) by using three different amine-boranes; ammonia-borane (AB; NH_3BH_3), methylamine-borane (MeAB; $CH_3NH_2BH_3$) and dimethylamine-borane (DMAB; $(CH_3)_2NHBH_3$) as reducing agent. Potassium dichromate ($K_2Cr_2O_7$) was selected as one of the demonstrative Cr(VI) compounds. It is well-known that the characteristics absorption peak of Cr(VI) is centered at 350 nm, which originates from the ligand (oxygen) to metal (Cr(VI)) charge transfer transition.[34–38] Hence the reduction of Cr(VI) can be monitored by UV–vis spectroscopy. Beforehand testing the catalytic activity of Ru@rGO catalyst, the catalytic reactivity of rGO as host material was examined in the catalytic reduction of Cr(VI) under identical conditions (*vide infra*). In the absence of Ru metal, the absorption intensity of Cr(VI) at 350 nm remains almost unchanged over 180 min, signifying that the host material rGO is catalytically inactive in the catalytic reduction of Cr(VI) and the reaction cannot proceed without Ru. Then, the catalytic reduction of Cr(VI) by using Ru@rGO in the presence of amine-boranes (AB, MeAB and DMAB) was surveyed under identical conditions (equimolar concentrations of [Ru], [$K_2Cr_2O_7$] and at 25 °C under air) and corresponding UV-vis spectra are given in

© 2020 Wiley-VCH Verlag GmbH & Co. KGaA, Weinheim

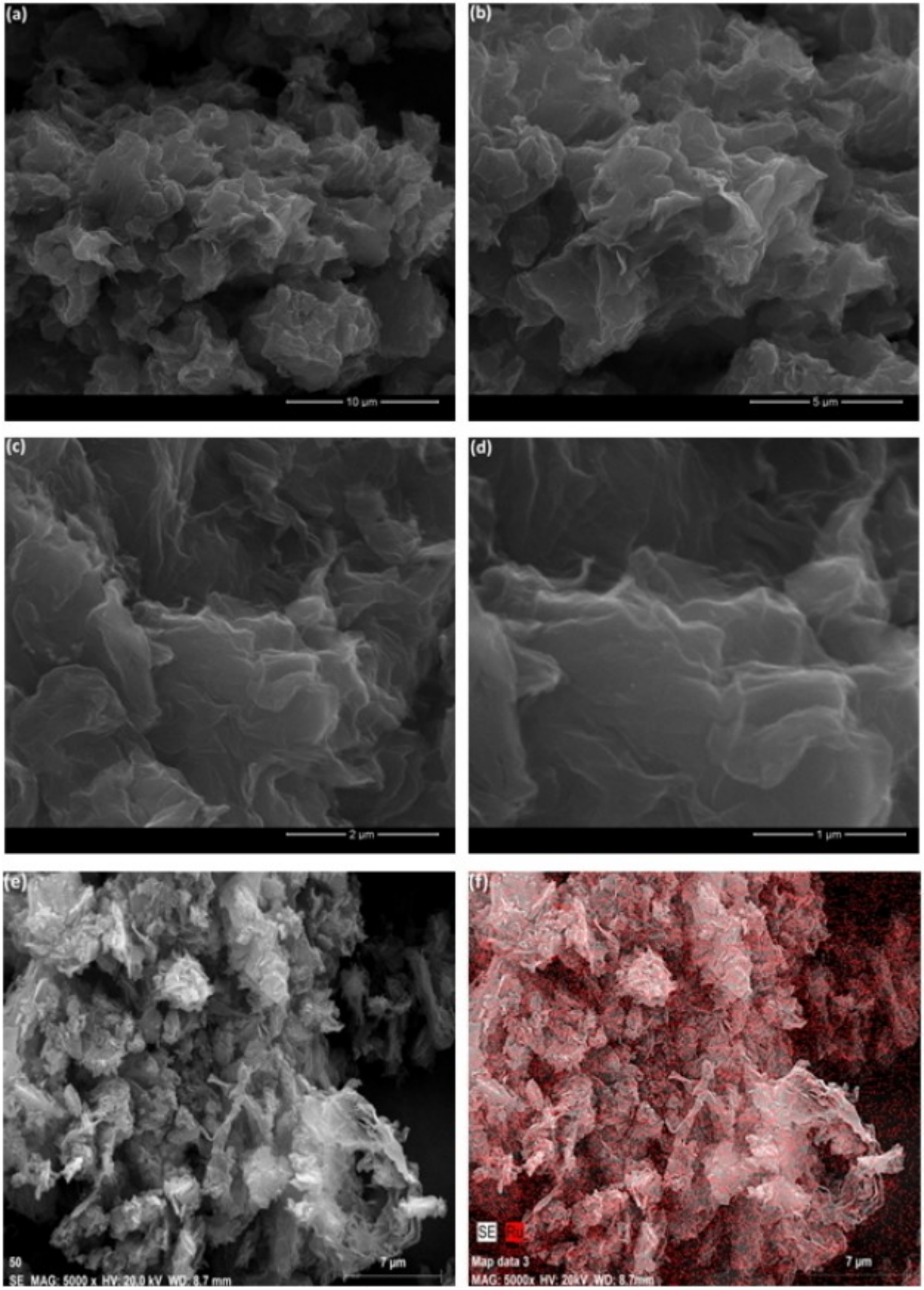


Figure 3. (a)-(e) Field emission scanning electron microscopy (FE-SEM) images of Ru@rGO taken at different magnification values and (f) SEM-EDX ruthenium mapping of Ru@rGO.

© 2020 Wiley-VCH Verlag GmbH & Co. KGaA, Weinheim

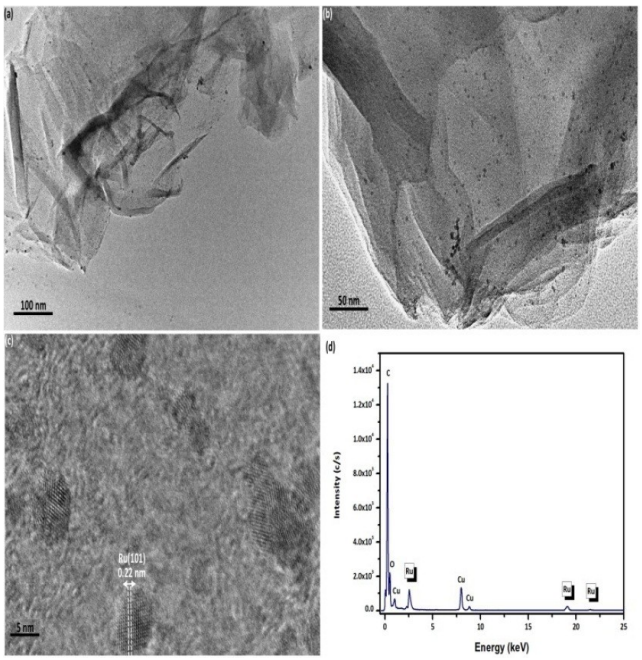


Figure 4. (a) and (b) TEM images of Ru@rGO at different magnifications, (c) HRTEM image of Ru@rGO, and (d) STEM-EDX spectrum of Ru@rGO.

Figure 5(a)-(c). As seen from these results, the highest activity was achieved in the presence of ammonia-borane, and the activity order of Ru@rGO in the presence of AB, MeAB, and DMAB was found to be AB > MeAB > DMAB. Actually, these results reflect the reactivity of amine-boranes, which was previously reported in the same order (AB > MeAB > DMAB).[39–42]

In order to confirm this reactivity, we also carried out a series of control experiments, in which the catalytic activity of Ru@rGO was examined in the catalytic hydrolysis of AB, MeAB, and DMAB (**4**-**6**) and the results of these experiments are given in Figure 5(d) in terms of equivalency of H_2 evolved versus time, which shows that (*i*) in the presence of the same amount of Ru@rGO only the catalytic hydrolysis of AB can occur at 100% conversion. As well as the volumetric measurement of the hydrogen evolution, the complete conversion of ammonia-borane to ammonium metaborate was also checked by comparing the intensities of signals of ammonia-borane and metaborate anion at $\delta = -23.9$ and 9.4 ppm, respectively, in the ^{11}B NMR spectra of the solution (**Figure S2**), (*ii*) the rate of hydrogen generation from Ru@rGO catalyzed AB, MeAB and DMAB was found to be in the order of AB > MeAB > DMAB that agrees with the rate of catalytic reduction of Cr(VI) in the presence of these amine-boranes. The rate of the catalytic reduction of Cr(VI) and the catalytic hydrogen generation plus their conversions in the presence of different amine-boranes are tabulated in Table 1.

Before starting to kinetic studies, to optimize catalytic reaction conditions, the effect of ruthenium loading was investigated in Ru@rGO catalyzed Cr(VI) reduction in the presence of AB. For this purpose, five Ru@rGO samples with

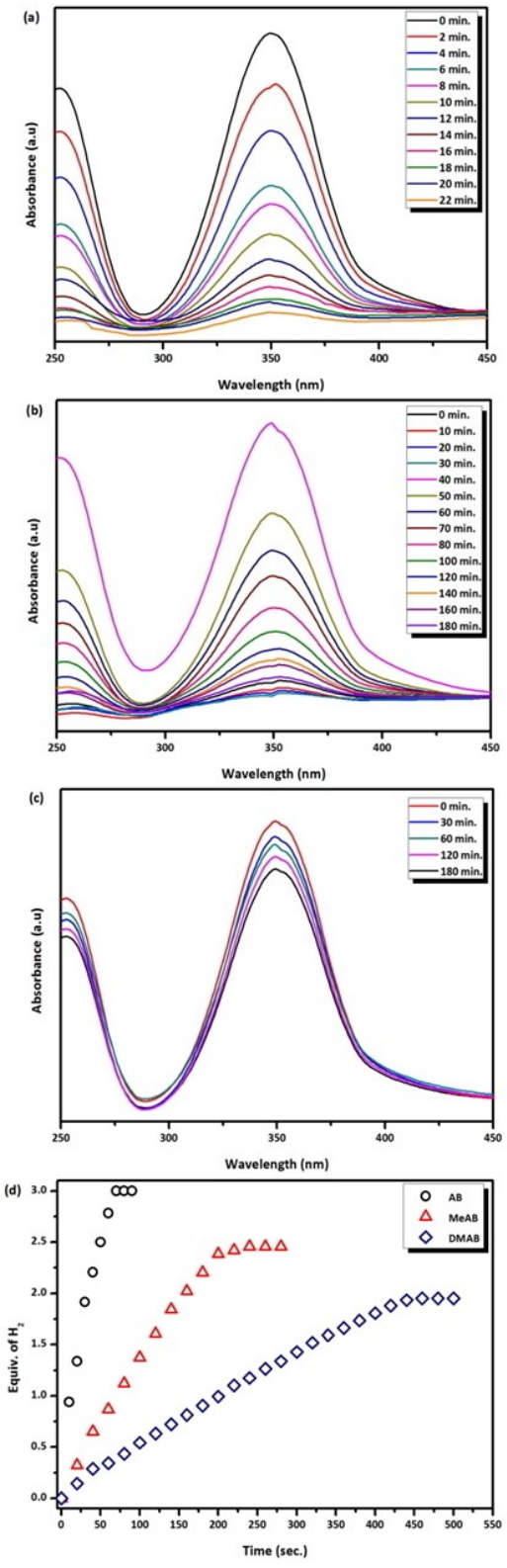


Figure 5. UV-vis spectra for Ru@rGO (10.0 mg, 1.2% wt Ru; 1.19 µol Ru) catalyzed reduction of aqueous (10.0 mL) $K_2Cr_2O_7$ (29.4 mg; 0.1 mmol $Cr_2O_7^{2-}$) in the presence of (a) ammonia-borane (31.8 mg; 1.0 mmol NH_3BH_3), (b) methylamine-borane (41.8 mg; 1.0 mmol $CH_3NH_2BH_3$), (c) dimethylamine-borane (58.9 mg; 1.0 mmol $(CH_3)_2NHBH_3$) at 25 °C, (d) the equivalency of H_2 generated versus time graph for Ru@rGO (30 mg, 1.2% wt Ru; 3.75 µmol Ru) catalyzed hydrolysis of aqueous AB, MeAB and DMAB (1.0 mmol in 10.0 mL H_2O) at 25 °C under air.

© 2020 Wiley-VCH Verlag GmbH & Co. KGaA, Weinheim

Table 1. The catalytic performance of Ru@rGO in terms of initial rates and conversions in the catalytic reduction of $Cr_2O_7^{2-}$ and the catalytic hydrolysis of amine-boranes (AB, MeAB, and DMAB) performed at 25 °C under air.

Reducing Agent	Catalytic Reduction of $Cr_2O_7^{2-}$		Catalytic Hydrolysis of Amine-Borane	
	Initial Rate[a]	Conversion (%)[b]	*Initial* Rate[c]	Conversion (%)[d]
AB (NH_3BH_3)	96	100	5.64	100
MeAB ($CH_3NH_2BH_3$)	33	92	0.98	82
DMAB ($(CH_3)_2NHBH_3$)	1.8	18	0.32	65

[a] Initial rate was defined as $\times 10^{-3}$ min.$^{-1}$ by considering the region where 20% conversion is achieved,[b] Conversion was calculated at $t = 180$ min.,[c] Initial rate was defined as the equivalency of H_2 generated/min. by considering the region where 20% conversion is achieved,[d] Conversion was calculated at $t = 500$ sec.

different ruthenium loadings (0.3, 0.8, 1.2, 2.6 and 4.8% wt Ru) were prepared by following the same methodology and tested as a catalyst in AB assisted Cr(VI) reduction under identical conditions. The results of these experiments in terms of initial rate-conversion versus % wt Ru loadings are given in Figure 6, which shows that the highest catalytic performance can be attained by using Ru@rGO catalyst with 1.2% wt Ru loading, which indicates that ruthenium nanoparticles in this sample are more accessible with respect to other tested Ru@rGO catalysts. The small size of the resulting ruthenium nanoparticles in Ru@rGO catalyst with 1.2% wt Ru loading may be another reason as the informative TEM image of Ru@rGO catalyst with 4.8% wt Ru loading is revealing that the formation of highly clumped ruthenium nanoparticles on the surface of rGO (**Figure S3**). It should also be noted that metal-free rGO was found to be catalytically inactive in AB assisted Cr(VI) reduction under identical conditions that followed for Ru@rGO catalysis.

The kinetic studies for Ru@rGO catalyzed Cr(VI) reduction in the presence of AB were performed depending on the catalyst ([Ru]), reducing agent ([AB]) concentrations and temperature. First, the effect of catalyst concentration ([Ru]) on the rate of Cr (VI) reduction was studied at the constant substrate ($[Cr_2O_7^{2-}]$), reducing agent ($[NH_3BH_3]$) concentrations and temperature. As

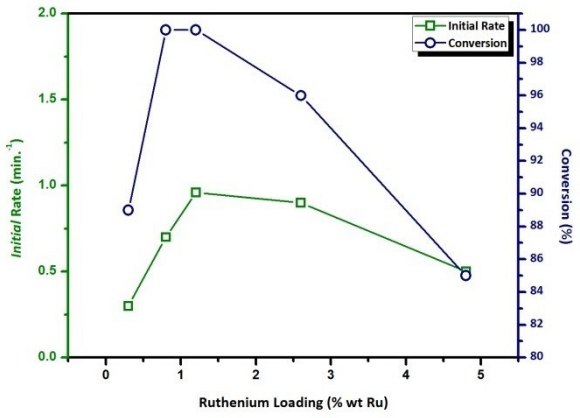


Figure 6. The initial rate-conversion versus ruthenium loading (% wt) graph for aqueous (10.0 mL) $K_2Cr_2O_7$ (29.4 mg; 0.1 mmol $Cr_2O_7^{2-}$) reduction in the presence of AB (31.8 mg; 1.0 mmol NH_3BH_3) by using Ru@rGO catalyst (in all 1.19 μol Ru) with various Ru loadings (0.3, 0.8, 1.2, 2.6 and 4.8% wt Ru) at 25 °C under air.

can be seen from UV-vis spectra of the reaction solution (**Figure S4**) at t = 2 min. (Figure 7(a)) for Cr(VI) reduction catalyzed by Ru@rGO catalyst with various ruthenium concentrations under identical conditions, the increase in ruthenium concentration enhances the rate of the catalytic Cr(VI) reduction. Figure 7(b) presents the remaining fraction of Cr(VI) ($[Cr(VI]/[Cr(VI)]_0$) versus time graphs for the catalytic reduction of Cr (VI) starting with different concentrations of Ru in Ru@rGO catalyst as one expected from a preformed catalyst, a nearly linear catalytic reduction starts without induction period and continues until to the end. The initial rates constants ($k_{initial}$) of catalytic reduction were determined from the linear portions of each plot in Figure 7(b) (0.048, 0.096, 0.180 min.$^{-1}$ for Ru concentrations of 0.089, 0.119 and 0.178 mM, respectively). Plotting the initial rate constants ($k_{initial}$) versus ruthenium concentration, both in logarithmic scales (Figure 7(c)), gives a straight line ($y = 1.46 + 1.83x$) with a slope of 1.83 indicating that Ru@rGO catalyzed reduction of Cr(VI) in the presence of AB is the second order with respect to the ruthenium concentration.

Then, to understand the effect of reducing agent concentration ([AB]) on the rate of Ru@rGO catalyzed Cr(VI) reduction a series of experiments were performed by varying AB concentrations (50, 100 and 200 mM) at constant substrate ($[Cr_2O_7^{2-}]$), catalyst ([Ru]) concentrations and temperature. UV-vis spectra of the reaction solution taken at t = 2 min. of these catalytic tests are given in Figure 8(a) (**Figure S5**) as seen from Figure 8(a) the rate of the catalytic Cr(VI) reduction increases by the increase of the reducing agent concentration. Fig. 8(b) shows the remaining fraction of Cr(VI) ($[Cr(VI]/[Cr(VI)]_0$) versus time graph for Ru@rGO catalyzed Cr(VI) reduction starting with various AB concentrations at 25 °C under air, and the initial rate constants ($k_{initial}$) were determined to be 0.045, 0.096 and 0.245 min^{-1} for AB concentrations of 50, 100 and 200 mM, respectively. The plot of $\ln k_{initial}$ versus ln[AB] graph given in Figure 8(c) has a straight line ($y = -10.81 + 1.03x$) with a slope of 1.03, which reveals that the Ru@rGO catalyzed Cr(VI) reduction in the presence of AB proceeds in first order with respect to ammonia-borane concentration.

Next, the effect of temperature on the rate of Ru@rGO catalyzed Cr(VI) reduction in the presence of AB was examined by performing the catalytic reaction at different temperatures (25, 35 and 45 °C) under air (**Figure S6**). Figure 9(a) depicts UV–vis spectra of the reaction solutions taken at t = 4 min. of these

© 2020 Wiley-VCH Verlag GmbH & Co. KGaA, Weinheim

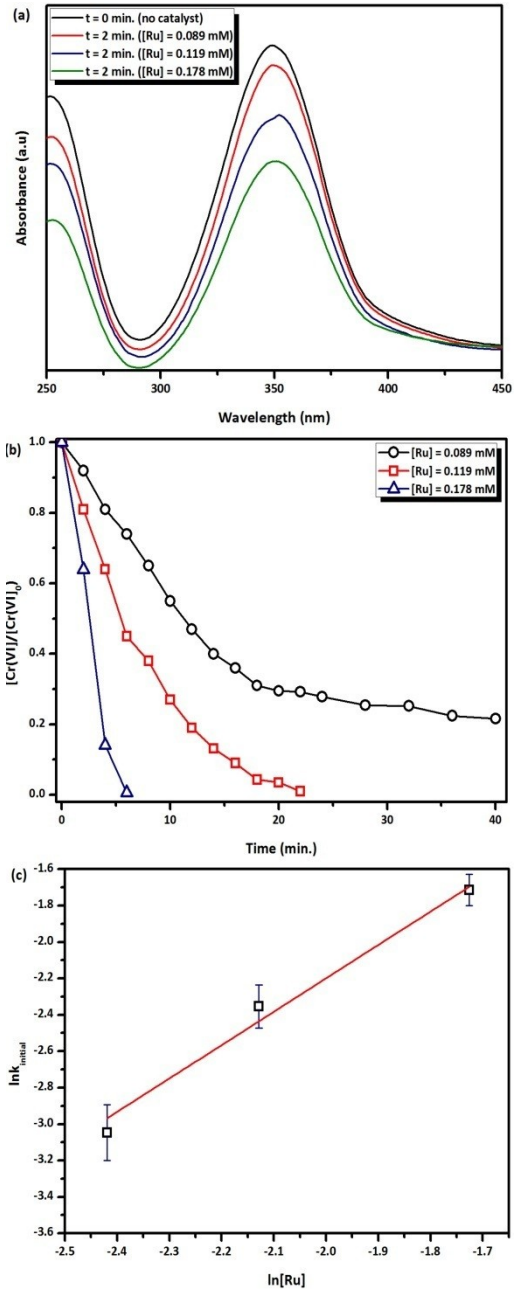


Figure 7. (a) UV-vis spectra (at t = 0 and 2 min.), (b) the remaining fraction of Cr(VI) ($[Cr(VI)]/[Cr(VI)]_0$) versus time graph, (c) the corresponding initial rate constants versus Ru concentration (both in logarithmic scales) graph for AB assisted Cr(VI) reduction (0.1 mmol $Cr_2O_7^{2-}$, 1 mmol AB in 10.0 mL H_2O) over Ru@rGO catalysts with different Ru concentrations (0.089, 0.119 and 0.178 mM) at 25 °C under air.

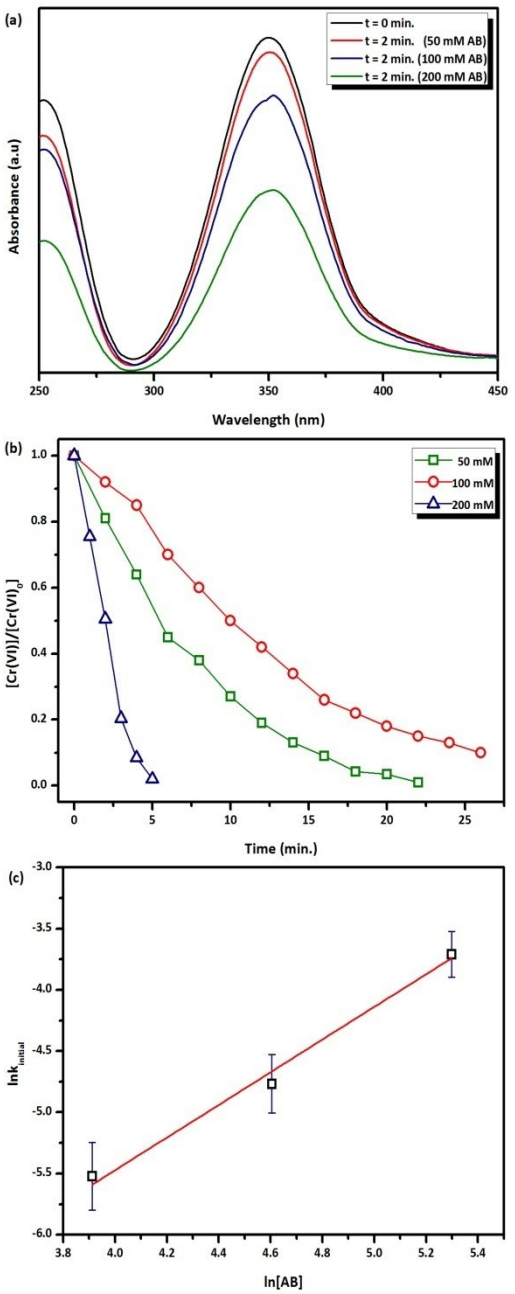


Figure 8. (a) UV-vis spectra (at t = 0 and 2 min.), (b) the remaining fraction of Cr(VI) ($[Cr(VI)]/[Cr(VI)]_0$) versus time graph, (c) the corresponding initial rate constants versus AB concentration (both in logarithmic scales) graph for Ru@rGO catalyzed Cr(VI) reduction (0.1 mmol $Cr_2O_7^{2-}$, 1.19 µol Ru in 10.0 mL H_2O) starting with various AB concentrations (50, 100, 200 mM) at 25 °C under air.

catalytic reductions as anticipatedly the temperature increase improves the rate of the catalytic Cr(VI) reduction. The remaining fraction of Cr(VI) ([Cr(VI]/[Cr(VI)]0] versus time graph for Ru@rGO catalyzed Cr(VI) reduction in the presence of AB at different temperatures is given in Figure 9(b), from which the activities at different temperatures in terms of initial turnover frequency values (TOF) were determined and found to be 7.6, 12.2 and 15.6 mol $Cr_2O_7^{2-}$/mol Ru.min at 25, 35 and 45 °C, respectively.

These activity values are higher than those previously obtained in formic acid assisted Cr(VI) reduction by using Pd@polymerNF (2.32 mol $Cr_2O_7^{2-}$/mol Pd.min at 50 °C),[19] Pd tetrapods (4.23 mol $Cr_2O_7^{2-}$/mol Pd.min at 50 °C),[20] PdPt bimetallic nanoparticles (1.66 mol $Cr_2O_7^{2-}$/mol metal.min at 45 °C),[43] Au@Pd (core@shell) nanoparticles (6.20 mol $Cr_2O_7^{2-}$/

© 2020 Wiley-VCH Verlag GmbH & Co. KGaA, Weinheim

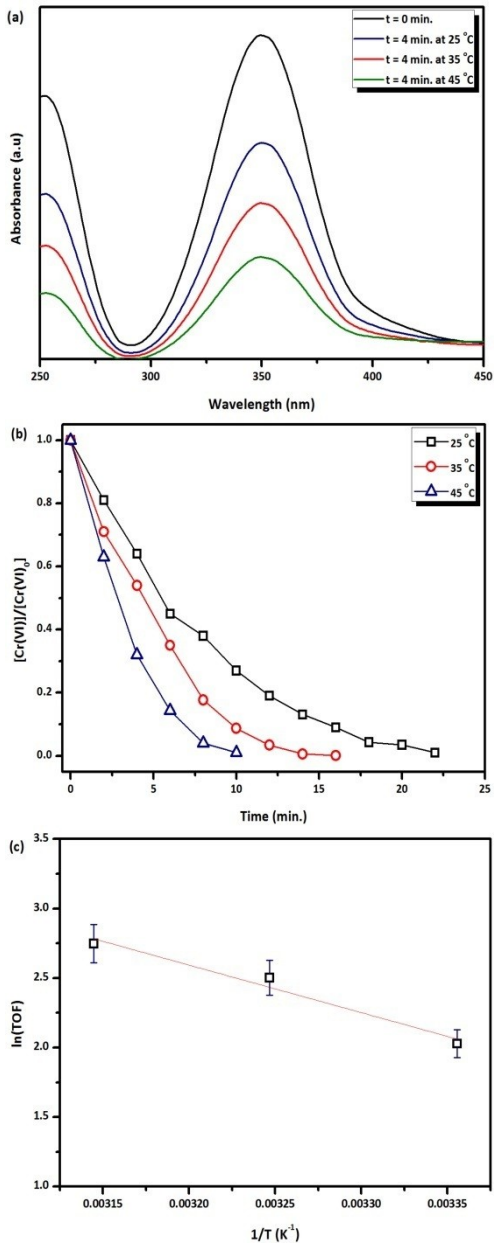


Figure 9. (a) UV-vis spectra (at t = 0 and 4 min.), (b) the remaining fraction of Cr(VI) ($[Cr(VI)]/[Cr(VI)]_0$) versus time graph for Cr(VI) reduction (0.1 mmol $Cr_2O_7^{2-}$, 1.19 μol Ru, 1.0 mmol AB in 10 mL H_2O) over Ru@rGO catalyst at different temperatures (25, 35 and 45 °C) under air, (c) the Arrhenius plot for Ru@rGO catalyzed Cr(VI) reduction in the presence of AB.

mol metal.min at 45 °C),[44] PdPt-ITO (9.52 mol $Cr_2O_7^{2-}$/mol metal.min at 50 °C),[45] PdCu nanocubes (7.12 mol $Cr_2O_7^{2-}$/mol metal.min at 40 °C)[46] and PdCu/ZIF-8 (4.22 mol $Cr_2O_7^{2-}$/mol metal.min at 35 °C).[47] In order to find the activation energy (Ea), the Arrhenius graph was constructed by plotting log TOF versus 1/T given in Figure 9(c), and from the linear Arrhenius behavior (y = 13.5 – 2917x), we calculated the activation energy to be 24.2 kJ/mol for Ru@rGO catalyzed Cr(VI) reduction in the presence of AB. To the best of our knowledge, this is the lowest value ever reported for catalytic Cr(VI) reduction in the presence of reducing agent; since the lowest Ea previously reported for catalytic Cr(VI) reduction is 25.9 kJ/mol,[15] in which formic acid was used as reducing agent.

Although, the detailed mechanistic studies are still performing in our research group, we think that the main mechanism of AB assisted Cr(VI) reduction is similar to that of FA assisted Cr(VI) reduction. In our system, AB undergoes catalytic hydrolysis and generates H_2, then, H_2 adsorbed on the surface of active metal nanoparticles subsequently reduces Cr(VI) to Cr (III) via an H_2 transfer pathway.[20,48, 49]

The catalytic stability of Ru@rGO was also examined by carrying out the reusability experiments in the catalytic reduction of Cr(VI) in the presence of AB. After the complete reduction of Cr(VI), Ru@rGO catalyst was isolated as a black powder bottled under argon atmosphere and kept in glove-box. Then, the isolated Ru@rGO catalyst was reused in the same catalytic reaction under identical conditions. This reused catalyst preserved 80% of its initial activity with a 90% conversion of Cr(VI) to Cr(III) even at 5th catalytic reuse (Figure 10). The TEM image of Ru@rGO catalyst harvested after 5th catalytic reuse (Figure10) shows the existence of clumped ruthenium nanoparticles on the surface of rGO, which explains the observation of minor decrease (~5%) in both activity and conversion. The adsorption of chromate ion onto the surface of

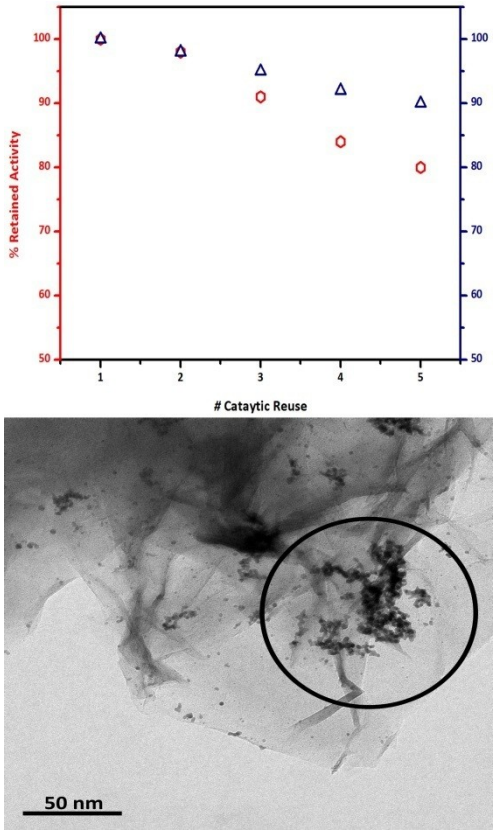


Figure 10. Retained catalytic performance (activity and conversion) versus the number of catalytic reuse for the reusability performance of Ru@rGO in the catalytic reduction of Cr(VI) in the presence of AB and TEM image of Ru@rGO harvested after 5th catalytic reuse; clumped ruthenium nanoparticles are labelled in a black circle.

© 2020 Wiley-VCH Verlag GmbH & Co. KGaA, Weinheim

catalytic material was also examined by ICP-OES analysis of Cr in the reused catalyst and we found that there is no Cr exists in the reused catalytic material. Moreover, the analysis of ruthenium content in the reused Ru@rGO catalyst and the aliquot taken from the reaction solution at 5th reuse by ICP-OES indicates that no leaching of ruthenium into the reaction solution. These results are indicative of the high stability of Ru@rGO catalyst against agglomeration and leaching throughout the catalytic reuse in the Cr(VI) reduction.

Conclusion

In this study, reduced graphene oxide (rGO) supported ruthenium nanoparticles (Ru@rGO) were prepared, characterized and used as heterogeneous catalyst in the reduction of Cr (VI) to Cr(III) in the presence of amine-boranes (AB, MeAB, DMAB) under mild conditions (at room temperature under air). Some of the major conclusions of this study can be summarized as follows:

(a) Ru@rGO catalyst was prepared by following a two-steps procedure comprising of a double-solvent method and chemical reduction technique with high reproducibility. The characterization of Ru@rGO by means of ICP-OES, P-XRD, XPS, HR-XPS, FE-SEM, TEM, HRTEM and STEM-EDX techniques revealed that the formation of well-dispersed 2.7 $\pm$ 0.9 nm ruthenium(0) nanoparticles on the surface of reduced graphene oxide,

(b) AB, MeAB and DMAB were used for the first time as reducing agent in the Ru@rGO catalyzed reduction of Cr(VI) to Cr(III) at room temperature. The catalytic tests reveal that Ru@rGO catalyzed Cr(VI) reduction in the presence of AB proceeds faster than those of performed in the presence of MeAB and DMAB, this result is in agreement with their strength of reducing ability (AB $>$ MeAB $>$ DMAB),

(c) Ru@rGO catalyzes Cr(VI) reduction in the presence of AB with an initial turnover frequency ($TOF_{initial}$) of 7.6 mol $Cr_2O_7^{2-}$/mol Ru.min even at room temperature and under air, this value is higher than the majority of the previously reported catalytic systems in which formic acid used as a reducing agent for Cr (VI) reduction,

(d) Testing the isolability and reusability of Ru@rGO showed that Ru@rGO catalyst retains 80% of its initial activity at 90% conversion in the catalytic reduction of Cr(VI) to Cr(III) even at 5th catalytic reuse. Moreover, ICP-OES and TEM analyses of disclosed that ruthenium nanoparticles display remarkable stability against to agglomeration and leaching throughout the reusability experiments,

(e) The quantitative kinetic studies depending on catalyst [Ru], reducing agent [AB] concentrations and temperature disclose that (*i*) Ru@rGO catalyzed Cr(VI) reduction in the presence of AB is second and first order with respect to Ru and AB concentrations, respectively, (*ii*) the activation energy of Ru@rGO catalyzed Cr(VI) reduction in the presence of AB was found to be 24.2 kJ/mol, which is the lowest Ea value reported for the catalytic reduction of Cr(VI) in the presence of reducing agents,

Supporting Information Summary

All experimental details, ^{11}B NMR, TEM, UV-vis spectroscopy results are given in the Supporting Information.

Acknowledgements

The authors thank to Yuzuncu Yil University Scientific Research Projects Coordination Unit (YYU-BAP) for the financial support to their project (FBA-2018-7143).

Conflict of Interest

The authors declare no conflict of interest.

Keywords: chromium(VI) · reduction · ruthenium · graphene oxide · amine-boranes

[1] M. Yadav, Q. Xu, *Chem. Commun.* **2013**, *49*, 3327–3329.
[2] S. K. Prabhakaran, K. Vijayaraghavan, R. Balasubramanian, *Ind. Eng. Chem. Res.* **2009**, *48*, 2113–2117.
[3] J. Kotas, Z. Stasicka, *Environ. Pollut.* **2000**, *107*, 263–283.
[4] L. H. Keith, W. A. Telliard, *Environ. Sci. Technol.* **1979**,*13*, 416–423.
[5] J. H. Chen, K. C. Hsu, Y. M. Chang, *Ind. Eng. Chem. Res.* **2013**, *52*, 11685–11694.
[6] S. Fendorf, B. W. Wielinga, C. M. Hansel, *Int. Geol. Rev.* **2000**, *42*, 691–701.
[7] M. Costa, C. B. Klein, *Crit. Rev. Toxicol.* **2006**, *36*, 155–163.
[8] M. Vainshtein, P. Kuschk, J. Mattusch, A. Vatsourina, A. Wiessner, *Water Res.* **2003**, *37*, 1401–1405.
[9] A. Zhitkovich, *Chem. Res. Toxicol.* **2011**, *24*, 1617–1629.
[10] H. Kyung, J. Lee, W. Choi, *Environ. Sci. Technol.* **2005**, *39*, 2376–2382.
[11] B. Hu, Y. Ai, J. Tin, T. Hayat, A. Alsaedi, L. Zhuang, X. Wang, *Biochar* **2020**, *2*, 47.
[12] N. S. Alharbi, B. Hu, T. Hayat, S. O. Rabah, A. Alsaedi, L. Zhuang, X. Wang, Front. Chem. Sci. Eng. https://doi.org/10.1007/s11705-020-1923-z.
[13] L. C. Hsu, S. L. Wang, Y. C. Lin, M. K. Wang, P. N. Chiang, J. C. Liu, W. H. Kuan, C. C. Chen, Y. M. Tzou, *Environ. Sci. Technol.* **2010**, *44*, 6202–6208.
[14] M. Celebi, M. Yurderi, A. Bulut, M. Kaya, M. Zahmakiran, *Appl. Catal. B* **2016**, *180*, 53–64.
[15] M. Yurderi, A. Bulut, M. Zahmakiran, M. Kaya, *App. Catal. B: Environ.* **2014**, *160*, 514–524.
[16] X. Gu, Z.-H. Lu, H.-L. Jiang, T. Akita, Q. Xu, *J. Am. Chem. Soc.* **2011**, *133*, 11822–11825.
[17] M. Yadav, Q. Xu, *Energy Environ. Sci.* **2012**, *5*, 9698–9725.
[18] A. Bulut, M. Yurderi, Y. Karatas, M. Zahmakiran, H. Kivrak, M. Gulcan, M. Kaya, *Appl. Catal. B* **2015**, *164*, 324–333.
[19] Y. Huang, H. Ma, S. Wang, M. Shen, R. Guo, X. Cao, M. Zhu, X. Shi, *ACS Appl. Mater. Interfaces* **2012**, *4*, 3054–3061.
[20] G. T. Fu, X. Jiang, R. Wu, S. H. Wei, D. M. Sun, Y. W. Tang, T. H. Lu, Y. Chen, *ACS Appl. Mater. Interfaces* **2014**, *6*, 22790–22795.
[21] F. Joo, *ChemSusChem* **2008**, *1*, 805–808.
[22] M. Grasemann, G. Laurenczy, *Energy Environ. Sci.* **2012**, *5*, 8171–8181.
[23] M. Zahmakiran, S. Ozkar, *Appl. Catal. B* **2009**, *89*, 104–110.
[24] I. B. Baguc, I. E. Ertas, M. Yurderi, A. Bulut, M. Zahmakiran, M. Kaya, *Inorg. Chim. Acta* **2018**, *483*, 431–439.
[25] S. Caliskan, M. Zahmakiran, F. Durap, S. Ozkar, *Dalton Trans.* **2012**, *41*, 4976–4984.
[26] A. Aijaz, A. Karkamkar, A. J. Choi, N. Tsumori, E. Roönnebro, T. Autrey, H. Shioyama, Q. Xu, *J. Am. Chem. Soc.* **2012**, *134*, 13926–13929.
[27] Q. L. Zhu, J. Li, Q. Xu, *J. Am. Chem. Soc.* **2013**, *135*, 10210–10213.
[28] R. J. White, R. Luque, V. L. Budarin, J. H. Clarka, D. J. Macquarrie, *Chem. Soc. Rev.* **2009**, *38*, 481–494.
[29] D. C. Marcano, D. V. Kosynkin, J. M. Berlin, A. Sinitskii, Z. Sun, A. Slesarev, L. B. Alemany, W. Lu, J. M. Tour, *ACS Nano* **2010**, *4*, 4806–4814.
[30] V. Singh, D. Joung, L. Zhai, S. Das, S. I. Khondaker, S. Seal, *Prog. Mater. Sci.* **2011**, *56*, 1178–1271.

© 2020 Wiley-VCH Verlag GmbH & Co. KGaA, Weinheim

[31] W. Vogel, L. Timperman, N. Alonso-Vante, *App. Catal. A: Gen.* **2010**, *377*, 167–173.
[32] N. Chakroune, G. Viau, S. Ammar, L. Poul, D. Veautier, M. M. Chehimi, C. Mangeney, F. Villain, F. Fiévet, *Langmuir* **2005**, *21*, 6788–6796.
[33] W. Chen, D. Ghosh, J. Sun, M. C. Tong, F. Deng, S. Chen, *Electrochim. Acta* **2007**, *53*, 1150–1156.
[34] M. Liang, L. Wang, X. Liu, W. Qi, R. Su, R. Huang, Y. Yu, Z. He, *Nanotechnology* **2013**, *24*, 245601–245610.
[35] A. Dandapat, D. Jana, G. De, *Appl. Catal. A* **2011**, *396*, 34–39.
[36] Y. Huang, H. Ma, S. Wang, M. Shen, R. Guo, X. Cao, M. Zhu, X. Shi, *ACS Appl. Mater. Interfaces* **2012**, *4*, 3054–3061.
[37] C. Yang, J. H. Meldon, B. Lee, H. Yi, *Catal. Today* **2014**, *233*, 108–116.
[38] C. Yang, A. K. Manocchi, B. Lee, H. Yi, *Appl. Catal. B* **2010**, *93*, 282–291.
[39] N. Zheng, J. Fan, G. D. Stucky, *J. Am. Chem. Soc.* **2006**, *128*, 6550–6551.
[40] S. B. Kalidindi, U. Sanyal, B. R. Jagirdar, *Inorg. Chem.* **2010**, *49*, 3965–3967.
[41] U. Sanyal, B. R. Jagirdar, *Inorg. Chem.* **2012**, *51*, 13023–13033.
[42] S. B. Kalindindi, U. Sanyal, B. R. Jagirdar, *ChemSusChem* **2011**, *4*, 317–324.
[43] M. Liang, R. Su, W. Qi, Y. Zhang, R. Huang, Y. Yu, L. Wang, Z. He, *Ind. Eng. Chem. Res.* **2014**, *53*, 13635–13643.
[44] X. Lia, C. Li, D. Xiang, C. Zhang, L. Xia, X. Liu, F. Zheng, X. Xie, Y. Zhang, W. Chen, *Appl. Catal. B* **2019**, *253*, 263–270.
[45] A. M. Mahar, A. Balouch, F. N. Talpur, Abdullah, Sirajuddin, A. Kumar, P. Panah, M. T. Shah, *Catal. Lett.* **2019**, *149*, 2415–2424.
[46] B. Qiao, J. Zhu, Y. Liu, Y. Chen, G. Fu, P. Chen, *CrystEngComm* **2019**, *21*, 3654–3659.
[47] Q. Zhao, L. Liu, R. Liu, L. Zhu, *Chem. Eng. J.* **2018**, *353*, 311–318.
[48] S. Yang, Q. Li, L. Chen, Z. Chen, Z. Pu, H. Wang, S. Yun, B. Hu, J. Chen, X. Wang, *J. Hazard. Mater.* **2019**, *379*, 120797.
[49] S. Yang, Q. Li, L. Chen, Z. Chen, B. Hu, H. Wang, X. Wang, *Chem. Eng. J.* **2020**, *385*, 123909.

Submitted: April 4, 2020
Accepted: May 31, 2020

© 2020 Wiley-VCH Verlag GmbH & Co. KGaA, Weinheim